DOI: 10.15480/882.9336

Eighth International Symposium on Marine Propulsors
smp'24, Berlin, Germany, March 2024

Ship URN mitigation by air injection: model-scale experiments and application to full-scale measurement data

Thomas Lloyd[1], **Frans Hendrik Lafeber**[1], **Johan Bosschers**[1]

[1]Maritime Research Institute Netherlands (MARIN), Wageningen, the Netherlands

ABSTRACT

It is recognised that continuous underwater radiated noise (URN) from shipping needs to be mitigated in order to minimise impact on marine animals. To this end there are numerous technical and operational URN mitigation measures, although extensive data concerning their effectiveness is not always available in the open domain. Examples of this include the so-called 'Masker' and 'Prairie' systems, designed to reduce machinery and propeller cavitation noise respectively by means of air injection. These types of systems are being studied within the EU Horizon 2020-funded project SATURN.

In this paper, we report model-scale sound measurement tests of both systems and demonstrate application of the measured data to a ship-scale test case. Two dedicated ship models were made based on a tanker hullform, with custom air injection systems developed. An overview of the model test campaign is reported, covering preparation, measurements and data analysis. After this, results of the full-scale application case are presented, including system power requirement estimation alongside URN abatement potential.

From the model tests URN reductions of up to about 22 dB and 12 dB were found for the Masker and Prairie-like systems respectively, although for the ship-scale application this is limited to about 10 dB at the vessel design speed.

Keywords

underwater radiated noise; cavitation; machinery; bubbles; air injection

1 INTRODUCTION

Underwater radiated noise (URN) from ships is receiving increasing attention for its adverse impacts on marine life (Duarte et al. 2021). Continuous noise from shipping - generated primarily by propeller cavitation and machinery - contributes to ambient sound levels in the oceans at a broad range of frequencies, with the potential to negatively affect a large number of species. Although there is currently no international regulation specifically addressing ship URN, in the European Union (EU) Member States are required to monitor ambient sound levels in the 63 Hz and 125 Hz decidecade frequency bands (EU 2017), with a procedure for determining threshold values for impact recently proposed (Technical Group on Underwater Noise 2022). Noise abatement is currently being addressed by multiple stakeholder groups, in anticipation of future regulation (Cruz et al. 2022). At international level, the International Maritime Organization (IMO) recently published revised guidelines for the reduction of URN from shipping (IMO 2023), while significant attention has been paid to monitoring and mitigation of ship URN within the Enhancing Cetecean Habitat and Observation (ECHO) Program (see e.g., Joy et al. 2019). The EU Horizon 2020 SATURN project is one initiative, addressing the sources, impacts and possible technical mitigation solutions. Within this project, one of the measures being studied by MARIN is air bubble injection for reduction of both propeller cavitation and machinery URN.

Although air injection systems for reducing noise and vibrations on board merchant ships have previously been studied (Hadler et al. 1984; Krueger et al. 2004), very little information is available in the open literature focusing on URN mitigation for similar vessels. Systems for this purpose have been developed for and used by a number of navies, meaning that almost no performance data is available in the public domain. Reduction of cavitation URN by air bubble injection was studied in the EU project SONIC however (Baudin & Mumm 2015). The aim of the present work was therefore to quantify the noise reduction potential of such air injection systems, in order to provide performance data for use in the design of (newbuild and retrofit) quiet ships.

For machinery noise abatement, the so-called 'Masker' system is used, which generates an air bubbles layer around the hull, thereby isolating the machinery noise sources on board the vessel from the surrounding water. In this case, the URN reduction is achieved by creating an impedance jump due to the bubbly mixture close to the hull. To reduce propeller cavitation noise, the 'Prairie' type of system was developed. This works by injecting air into the cavitation through holes in the leading edges of the propeller blades. The non-condensable gas dampens the collapse of the cavity, which is the main noise generation mechanism. In this work, we studied a solution whereby air is injected

from upstream of the propeller disc, which we refer to as a 'Prairie-like' system. Sketches of the two systems applied to a cargo vessel are shown in Figure 1.

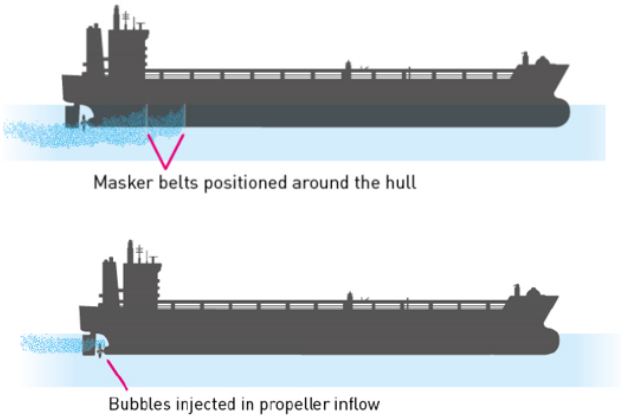

Figure 1: Schematic representations of Masker and Prairie-like systems applied to a cargo vessel.

This paper reports the model test campaigns performed at MARIN for studying the performance of the Masker and Prairie-like systems, followed by an example application of the processed measurement data to a full-scale test case. Although several different types of measurements have been performed for each system, we focus here on the URN results. More details of the complete model test programme are given in Lloyd et al. (2024).

2 MODEL TESTS

2.1 Ship geometry

A common hullform geometry was selected for the scale model tests of both air injection systems. The chosen ship was a 7000 DWT tanker, previously used in the EU Streamline project (Dymarski et al. 2011) and not subject to restrictions in sharing of the hull and propeller geometries or associated results. She has a design speed of 14 knots and is equipped with a single fixed-pitch propeller. Main particulars of the hull and propeller are given in Table 1.

Table 1: Streamline tanker principal particulars.

Particular	Symbol	Value	Unit
Length between perp.	L_{bp}	94.00	m
Beam	B	15.42	m
Draught (forward/aft)	T	6.01	m
Block coefficient	C_b	0.762	-
Propeller diameter	D	3.85	m
Number of blades	Z	4	-
Pitch at $0.7R$	$P_{0.7}/D$	1.00	-
Exp. area ratio	A_E/A_0	0.579	-

Two dedicated scale models were developed for the present work, due to the differing requirements of the measurements for each air injection system. This also resulted in two different scale factors (λ), with 12.00 used for the Masker system and 12.83 for the Prairie-like system.

2.2 Experimental design and execution

2.2.1 Test facility

All tests were performed in MARIN's Depressurised Wave Basin, which measures 240 m x 18 m x 8 m. The ambient air pressure in the facility can be reduced in order to obtain cavitation number similarity in combination with Froude scaling of the model speed and propeller rotation rate. This was applied when testing the Prairie-like system, but was not required for the Masker system, with these tests performed at atmospheric pressure conditions. Furthermore, all tests were performed in calm water conditions with the models towed straight ahead at even keel. A dedicated silent towing carriage (Bosschers et al. 2013) was used for the URN measurements, with all other measurements made using the main towing carriage. Sound was measured using hydrophones mounted on a mast at the centre of the basin, which the models sail over. Results from a single hydrophone - located on the tank centreline - are presented in this work. More details of the test facility and setup for URN measurements can be found in Lloyd et al. (2018).

2.2.2 Masker system

In order to imitate ship machinery noise, a simplified scaled metal midship section was developed and attached to wooden fore and aft sections to form the ship model. The metal section was excited by a shaker which was fed with white noise signals, with the aim of achieving a broadband excitation of the ship-like structure. A low-pass (LP) filtered signal was used for some tests with the aim of increasing the response of the structure - and therefore signal-to-noise ratio of the tests - at low frequencies. No propeller was included since the focus was only on machinery noise. Air was injected along the sides and keel of the model through porous hoses recessed into the hull just upstream of the metal midship section. The model was painted blue in order to improve the quality of high-speed camera observations of the bubble layer, which were made in keel and beam aspect. Full details can be found in Lloyd et al. (2023).

In addition to URN measurements, a custom bubble measurement system was developed in-house. This system was able to quantify the time-averaged normal-wall air void fraction distribution, at discrete girthwise and streamwise positions under the metal midship section. More information on the development and application of this system can be found in Klinkenberg et al. (2023). A photograph of the Masker scale model, showing both the air injection system and bubble measurement system, is provided in Figure 2.

Firstly, observations of the bubble layer were made in order to select appropriate air flow rates at several model speeds. Following this, the URN measurements were performed, in which the model speed, air flow rate and shaker signal were varied. Finally, for selected conditions, the characteristics of the bubble layer were measured at three stations.

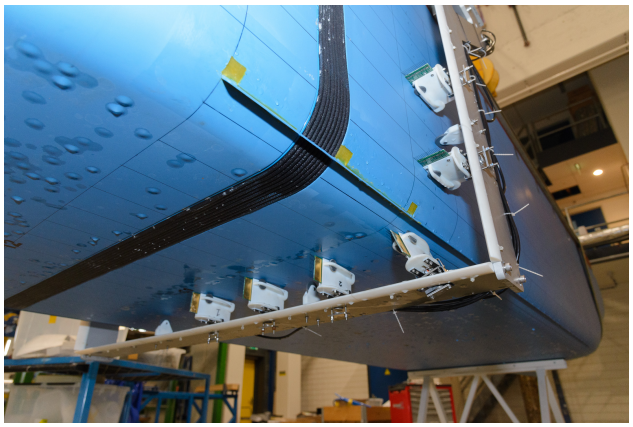

Figure 2: Air injection (Masker) system and bubble measurement system developed for present model tests: perspective view from port side below the keel.

2.2.3 Prairie-like system

A Prairie-like system was developed with air injected through needles mounted in a duct located upstream of the propeller disc. The duct was designed (using computational fluid dynamics) to have a minimal effect on propeller performance, and sized and oriented with the aim of having bubbles enter the cavity close to the propeller tip. The final design was manufactured using 3D printing, with air supplied to the upper and lower halves independently via two mass flow controllers.

The model was prepared for cavitation and URN measurements following MARIN's standard procedures, with the propeller painted blue and sandgrain roughness applied to the leading edges of the propeller blades. Figure 3 gives an impression of the Prairie-like system.

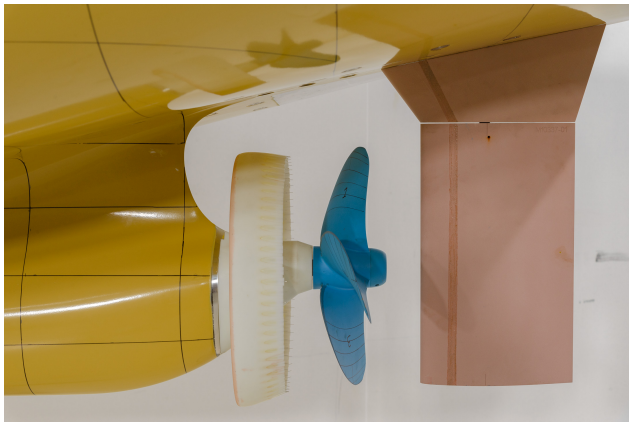

Figure 3: Prairie-like system developed for present model tests. Air is injected from needles mounted in the trailing edge of the duct upstream of the propeller rather than from holes in the propeller blade leading edges (as in the original Prairie system).

Observations were performed first, using high-speed cameras. Tests were performed for four different combinations of propeller thrust coefficient and cavitation number, designed to cover low and high propeller loading conditions, with varying forms and degrees of cavitation present. This was done intially without air injection for baseline performance assessment, after which a range of air flow rates were used. Propeller thrust and torque, and hull pressure fluctuations, were also measured. The test conditions were subsequently repeated to measure URN. Lastly, shadowgraphy measurements were made for selected test conditions (air flow rates and model speeds), using a dedicated high-speed camera setup from inside the model, with the aim of quantifying the bubble size distribution generated by the injectors. Further details can be found in Lloyd et al. (2024).

2.3 Data analysis

2.3.1 Source levels

Since the measurements of the Prairie-like system closely resembled other typical URN setups tested in the DWB, standard data processing procedures could be used to estimate the source levels (SLs). This involves windowing the measurement such that only data points within the reverberation radius of the facility are included, after which this data is segmented and corrected for propagation loss (including the Lloyd's mirror effect), before correcting for background noise and averaging over all segments to obtain the final (model-scale) SL. Scaling follows International Towing Tank Conference (ITTC) Recommended Procedures (ITTC 2017). Further details can be found in Lloyd et al. (2018).

In the case of the Masker system, a modified procedure was adopted as the noise source being studied was quite different from propeller cavitation noise. Since machinery noise is not monopole in nature, no Lloyd's mirror correction was applied. In addition, no scaling of the derived source levels was carried out, assuming that the measured sound level reduction was primarily a function of the bubble layer void fraction and that the sound was generated by a generic representative broadband source (Lloyd et al. 2023).

2.3.2 Air injection system performance

The performance of the air injection systems in terms of change in sound levels is computed as the difference between the predicted source levels without and with the system turned on. For the Masker system, this is termed the insertion loss (IL), since the mitigation device is located between source and receiver, and the source itself is not reduced in magnitude. For the Prairie-like system, injecting air directly into the cavity means that the source strength does reduce, hence we refer to this as the source level attenuation (SLA). These two quantities are simply defined as the difference in SL between the test condition with the system switched off and switched on.

The difference between IL and SLA may appear to be largely semantic, with both quantities derived in the same way, even if the URN reduction mechanisms are different. Despite this, the distinction in terminology is important since the 'source level' at one metre when the Masker system is switched on does not represent the strength of the sound source; it can be thought of as a distance-corrected sound pressure level. This is not relevant for the URN performance quantification however,

which for both systems is based purely on the difference in the processed sound levels between tests with and without air injection.

2.4 Exemplar model test results

This section contains a brief overview of the URN results and related bubble observations. For full results the reader is referred to Lloyd et al. (2024).

2.4.1 Masker system

A high-speed camera observation of the Masker air bubble layer in keel aspect is shown in Figure 4. The model speed (V_m) is 2.13 m/s - equivalent to the ship service speed - and the air flow rate (Q_m) was 3.75×10^{-3} m^3/s. Overall a rather uniform bubble layer can be seen. The bubbles were also observed to convect reasonably evenly over the sides of the hull for this condition.

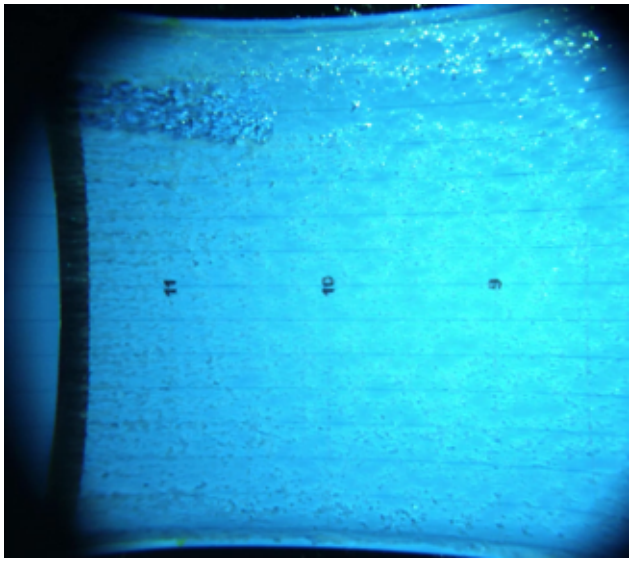

Figure 4: Example bubble layer observation for Masker system. Camera mounted in keel aspect on hydrophone mast, with model sailing from right to left.

A corresponding SL spectra comparison is presented in Figure 5, with the associated IL shown in Figure 6. There is a clear SL reduction across most of the frequency range, resulting in an IL of up to 21 dB for this case. Despite this, at certain frequencies the measured mitigated source level is equal to the source level with bubble injection only. The derived IL is limited at these frequencies, primarily due to the lower response of the metal midship section. The blue spectrum in Figure 5 exhibits several distinct peaks, between which the SL is up to 25 dB lower, thereby reducing the signal-to-noise (SNR) ratio at these frequencies. This artefact is denoted by dashed faded lines in Figure 6, indicating that the true IL may be higher. Another point of note is the small increase in SL (negative IL) which was obtained across multiple test conditions for a limited frequency range (between about 300 Hz to 400 Hz in this case). It is hypothesised that this may be related to bubble resonance (Lloyd et al. 2023).

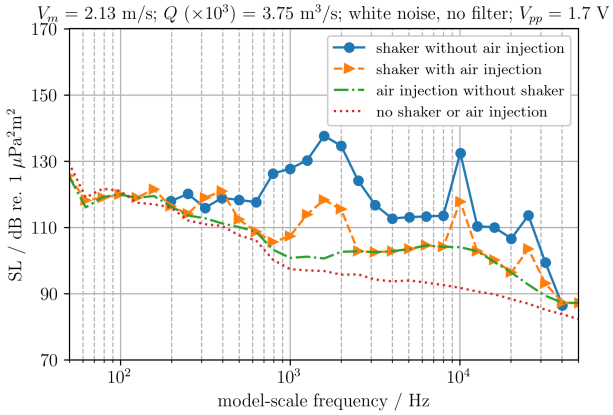

Figure 5: Example processed decidecade bandwidth source level spectra for Masker system.

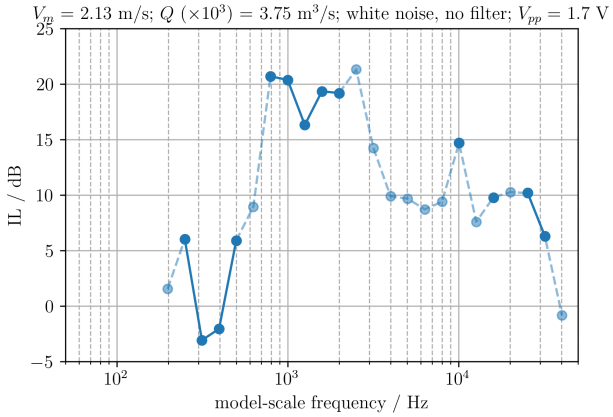

Figure 6: Example insertion loss spectrum for Masker system. Dashed lines indicate frequencies for which the predicted insertion loss is limited by the signal-to-noise ratio of the measurements.

2.4.2 Prairie-like system

The test conditions for the Prairie-like system are defined in terms of the propeller thrust coefficient and cavitation number:

$$K_T = \frac{T}{\rho n^2 D^4} \tag{1}$$

and

$$\sigma_n = \frac{2(p_{atm} + \rho g h_{\text{shaft}} - p_v)}{\rho n^2 D^2}, \tag{2}$$

as well as the air flow rate. In Eq. 1, T is the mean propeller thrust, ρ the water density and n the propeller rotation rate in Hertz. In Eq. 2, p_{atm} and p_v are the atmospheric and vapour pressures respectively, g acceleration due to gravity and h_{shaft} the (reference) propeller shaft immersion.

An example cavitation and bubble observation for the Prairie-like system can be seen in Figure 7, for which $K_T = 0.274$, $\sigma_n = 0.259$ and $Q_m(\times 10^6) = 25.0$ m^3/s. Here (as for most of the tests performed) air was only injected from the upper half of the duct, with the aim of bubbles entering the cavity close to the top position, where the cavity was at its largest, and just before the primary collapse occurred.

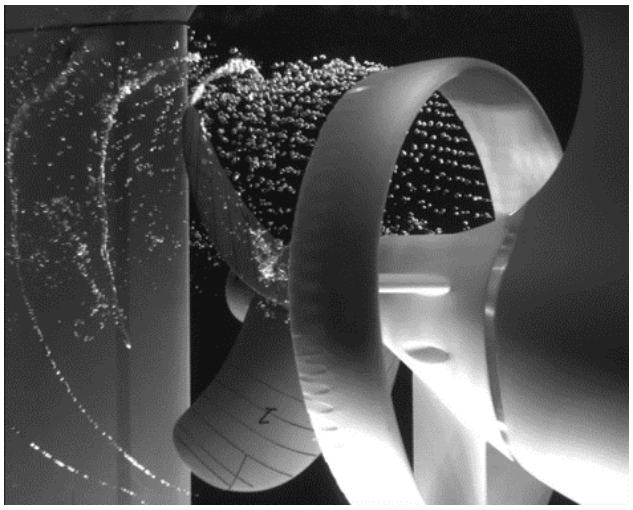

Figure 7: Example cavitation and bubble observation for Prairie-like system.

Source level spectra for this test condition are shown in Figure 8, where (in contrast to the Masker system) the background noise spectrum is the same both with and without air injection, as a much smaller amount of air is injected. The corresponding SLA is plotted in Figure 9. Although the SNR was not sufficient at some frequencies - resulting in data points being omitted - modest to large reductions in source level are seen at most of the remaining frequencies. The largest reduction in all cases is found for the cavitation 'hump' (here centred at 40 Hz), indicating that the non-condensable gas is able to dampen the main cavity collapse. At lower frequencies (below 30 Hz here), the SL increases when air injection is applied, which could be due to the increased size (thickness) of the cavity when it contains air.

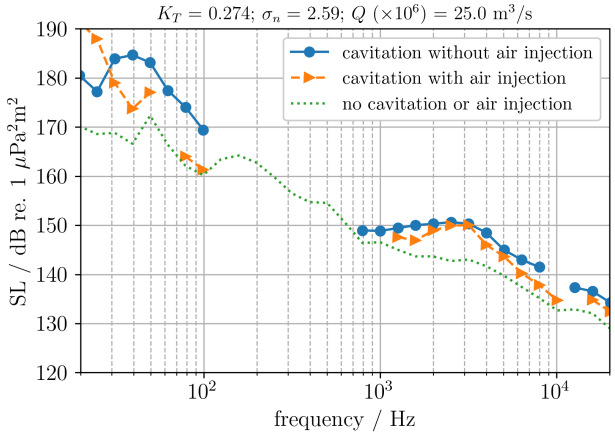

Figure 8: Example processed full-scale decidecade bandwidth source level spectra for Prairie-like system.

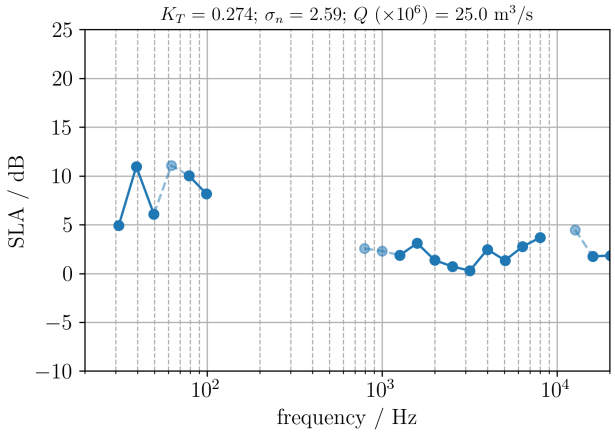

Figure 9: Example full-scale source level attenuation spectrum for Prairie-like system.

3 APPLICATION TO FULL-SCALE MEASUREMENT DATA

We now present the application of results such as those presented in Section 2 to a case of measured ship URN.

3.1 Test case description

A test case from the open literature was selected (Arveson & Vendittis 2000). It concerns the bulk cargo ship M/V Overseas Harriette, built in 1978, with an overall length of 173 metres. The vessel is propelled by a 4.9 metre diameter fixed-pitch propeller directly driven by a 8.4 MW two-stroke diesel engine. Auxiliary power is provided by a diesel generator. Decidecade radiated noise level (RNL)** spectra measured in keel aspect are available for five test conditions. Three of these were selected in the present work, corresponding to the lowest, middle and highest ship speeds tested. The RNL spectra for these speeds are shown in Figure 10.

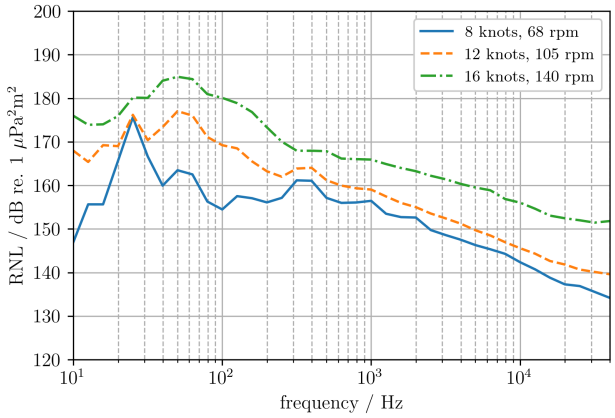

Figure 10: Radiated noise level spectra for full-scale application case. Data taken from Arveson & Vendittis (2000). Legend indicates vessel operating condition in terms of ship speed and propeller rotation rate.

The three conditions show clear differences in terms of spectral characteristics, which can be interpreted as being due to the increasing contribution of propeller cavitation noise with vessel speed. At 8 knots, machinery tonals

**Spherical spreading loss was applied as opposed to calculating the propagation loss.

dominate the spectrum at low frequencies (about 25 Hz) while the hump centred between 300 Hz and 400 Hz may be caused by the diesel generator. Note that the propeller is not cavitating at this speed, with the cavitation inception speed (CIS) reported to be 10 knots (Arveson & Vendittis 2000). For 12 knots, the machinery noise contributions at the aforementioned frequencies are still visible, yet there is a broadband increase in RNL, particularly centred between 50 Hz and 60 Hz, which can be attributed to the cavitating tip vortex. At 16 knots, this characteristic hump has increased in terms of both level and width, while cavitation noise dominates the spectrum at all frequencies, due to this source mechanism having a higher speed-dependency than machinery noise.

Table 2 summarises the three test conditions and the model test data selected for application to each. For the Masker data, the highest measured insertion loss was used, which was obtained for the highest model speed and air flow rate tested. In this we assume that the power requirement of the air injection system (at ship scale) is not a deciding factor when selecting the air flow rate. Furthermore, part of the variation in IL as a function of model speed was attributed to scale effects in the model tests (Lloyd et al. 2024) and we therefore do not try to match the (scaled) speed from the model tests with that from the application case. On the other hand, for the Praire-like system, source level attenuation data were selected by taking the model-scale test conditions having the closest correspondence (in terms of ship speed and propeller rotation rate) with those of the ship-scale case. The ship speeds match reasonably well across both conditions. For the 16 knots case, although the speed and rotation rate differ by about 14 %, the propeller apparent advance ratios $J_V = V_s/(n_s D)$ are very similar (0.72 and 0.70 for the M/V Overseas Harriette and Streamline tanker respectively). The main reason for trying to match the test conditions is that the performance of the Prairie-like system was observed to be somewhat dependent on the propeller loading condition (Lloyd et al. 2024). No Prairie-like data is applied at 8 knots since the propeller is not cavitating.

Table 2: Test conditions for application case and corresponding selected model test conditions.

Full scale			Masker			Prairie		
Condition	V_s kn	N_s rpm	V_s kn	Signal type	$Q_m(\times 10^3)$ m^3/s	V_s kn	N_s rpm	$Q_m(\times 10^6)$ m^3/s
Low speed	8	68	14	no filter	6.25	-	-	-
Middle speed	12	106	14	no filter	6.25	12	108	16.7
High speed	16	140	14	no filter	6.25	14	160	25.0

3.2 Data processing

The IL and SLA spectra used for the present analysis are shown in Figure 11 and 12.

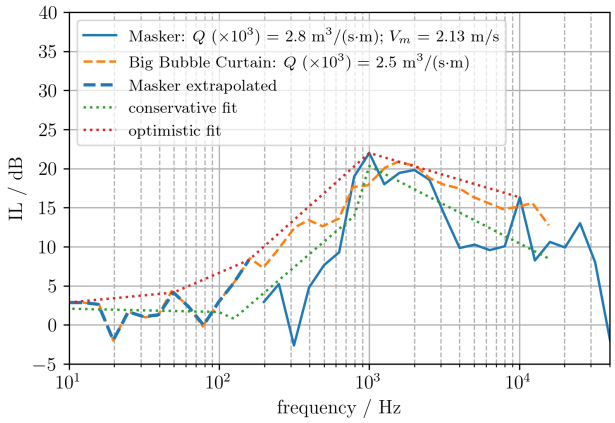

Figure 11: Masker system insertion loss for selected operating condition. Comparison data for Big Bubble Curtain taken from Bellmann (2014).

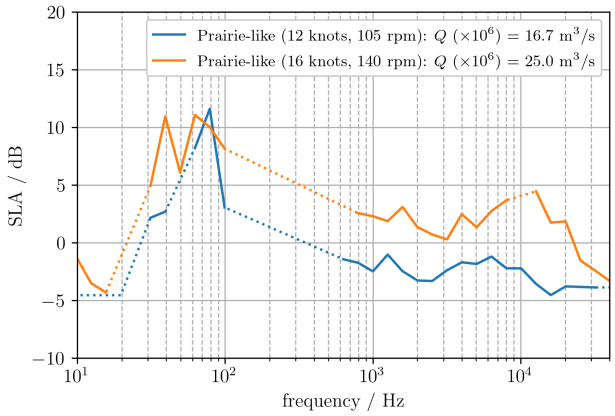

Figure 12: Prairie-like system source level attenuation for two operating conditions. Dotted lines indicate data filling by linear interpolation.

Prior to applying the data to the ship-scale measured RNL some further processing was applied to the insertion loss spectra. The IL obtained from the present measurements is compared to data from literature for a 'Big Bubble Curtain' (BBC), used to mitigate noise from offshore pile-driving (Bellmann 2014). Data for the BBC at the closest air flow rate to the selected Masker test condition was chosen, where the flow rate of the Masker data was scaled to the same units as used by Bellmann (2014) for reporting the BBC results; that is, the volumetric flow rate per metre injector.

Overall, a good agreement is seen between the two datasets, with a similar trend in terms of spectral shape and level across much of the frequency range presented. As discussed in Section 2, the magnitude of the IL obtained from the present measurements was sometimes limited by the achievable SNR. The comparison with the BBC data seems to reinforce this observation, with a very good agreement seen at frequencies for which a strong

resonant response of the scaled metal midship section was measured. This motivated two further data processing steps before applying the IL data to the ship RNLs. Firstly, the missing IL data at low frequencies was extrapolated using data from the BBC (dashed blue line in Figure 11). Following this, two data fits were made in order to obtain a smoother IL spectrum: a linear regression in three frequency ranges using all data points; and a linear fit between the peaks of the Masker IL data. These two data fits therefore represent 'conservative' and 'optimistic' estimates of the Masker system performance respectively (see Figure 11).

Data fitting was not performed for the SLA data since similar artefacts from the model tests were not present in the results. However, in order to have continuous data across all decidecade frequency bands, the missing data points were approximated by linear interpolation. This is indicated by dotted lines in Figure 12.

For the present application case, it is necessary to estimate the contribution of propeller cavitation noise to the total measured RNL spectrum. This can be done by:

$$L_{RN,cav}\,(f)\,[dB] = 10\log_{10}\left(10^{\frac{L_{RN,total}(f)}{10}} - 10^{\frac{L_{RN,mach}(f)}{10}}\right), \quad (3)$$

where $L_{RN,total}$ is the RNL as reported in Arveson & Vendittis (2000) and $L_{RN,mach}$ is the machinery noise, taken as the 8 knots condition. Subsequently, the mitigated RNL for each source mechanism can be computed as:

$$L_{RN,cav,air}\,(f)\,[dB] = L_{RN,cav}\,(f) - SLA\,(f) \quad (4)$$

and

$$L_{RN,mach,air}\,(f)\,[dB] = L_{RN,mach}\,(f) - IL\,(f), \quad (5)$$

following which the total mitigated RNL is obtained as:

$$L_{RN,total,air}\,(f)\,[dB] = 10\log_{10}\left(10^{\frac{L_{RN,cav,air}(f)}{10}} + 10^{\frac{L_{RN,mach,air}(f)}{10}}\right). \quad (6)$$

The overall change in RNL including the mitigation effect of both Masker and Prairie-like systems is given by:

$$\Delta L_{RN,total}\,(f)\,[dB] = L_{RN,total,air}\,(f) - L_{RN,total}\,(f). \quad (7)$$

3.3 URN mitigation results

Results are presented in terms of the reference and mitigated RNL, as well as the change in RNL, for each of the three speeds considered. Figure 13 shows the RNL spectra for the three ship speeds considered. For the 12 knots and 16 knots cases, the effect of the systems on the cavitation and machinery source mechanisms separately is also presented, in Figure 14.

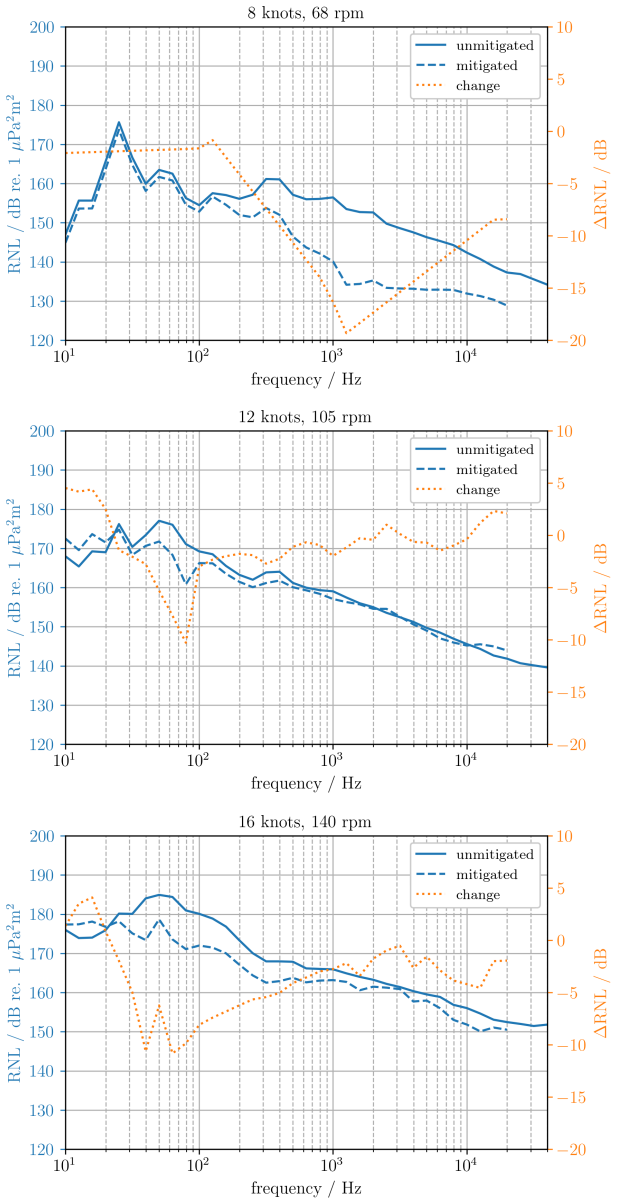

Figure 13: Unmitigated and mitigated radiated noise level combining propeller cavitation and machinery noise, for three operating conditions: 8 knots (top); 12 knots (middle); and 16 knots (bottom). Left-hand y-axis shows RNL and right-hand y-axis gives the change in RNL. 'Conservative' data fit for Masker insertion loss used.

Radiated noise level reductions of almost 20 dB are found for the non-cavitating condition reducing to about 10 dB above CIS. For the lowest speed, this is centred at 1 kHz, where the Masker system is most effective, with little effect at low frequencies where machinery noise tonals are present. For the other two speeds, the contribution of machinery noise to the total RNL is smaller, meaning the effect of the Masker system does not contribute as much to the change in RNL. At 12 knots, the Prairie-like system leads to increased RNL in the frequency range where the Masker system works best, meaning that any benefit is cancelled out. For 16 knots, cavitation noise

dominates at almost all frequencies, making the Masker system ineffective. As expected, the Prairie-like system is most effective at frequencies centred around the cavitation hump peak frequency. The RNL increases at very low frequencies (< 20 Hz) while changes at higher frequencies can be positive or negative depending on the case, but mainly lie within about 3 dB.

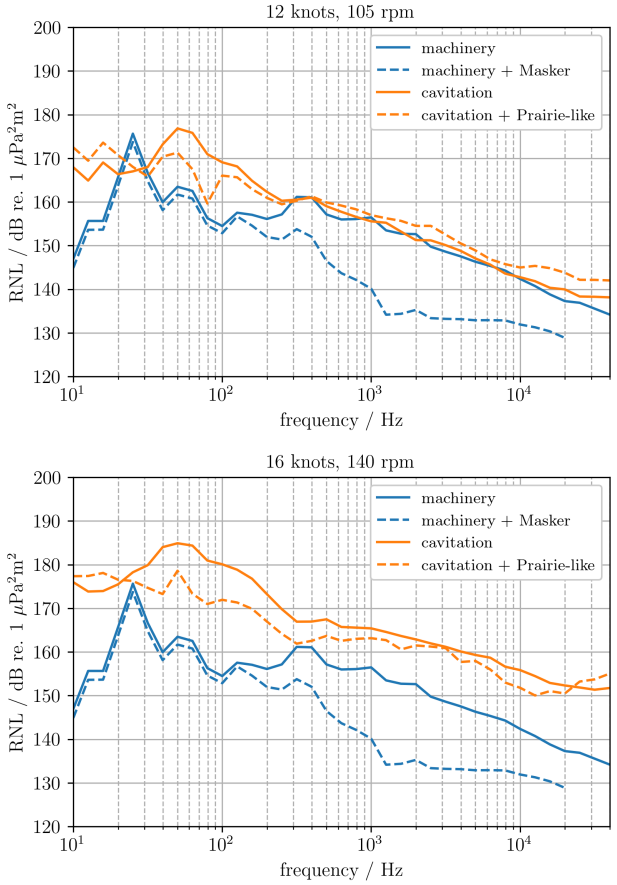

Figure 14: Unmitigated and mitigated radiated noise level when applying appropriate air injection system to propeller cavitation and machinery noise source mechanisms separately, for two operating conditions: 12 knots (top); and 16 knots (bottom). 'Conservative' data fit for Masker insertion loss used.

A summary of the estimated changes in RNL for all three ship speeds is shown in Figure 15, which includes results for both 'conservative' and 'optimistic' performance of the Masker system. The optimistic scenario results in an increase of the peak change in RNL from 19 dB to 22 dB for the 8 knots case, while the difference between the two modelling approaches is much smaller when applied to the two higher speeds, since the Masker system is less effective in reducing the total RNL for these cases.

3.4 Air flow rate and power requirement

An estimate should also be made of the required air flow rate when applying the air injection systems on board ships, such that compressor power requirement can be specified. Here we present arguments for scaling of the air flow rates used during the model tests to full scale, for both Masker and Prairie-like systems. Sketches of both systems including the important parameters are shown in Figures 16 and 17.

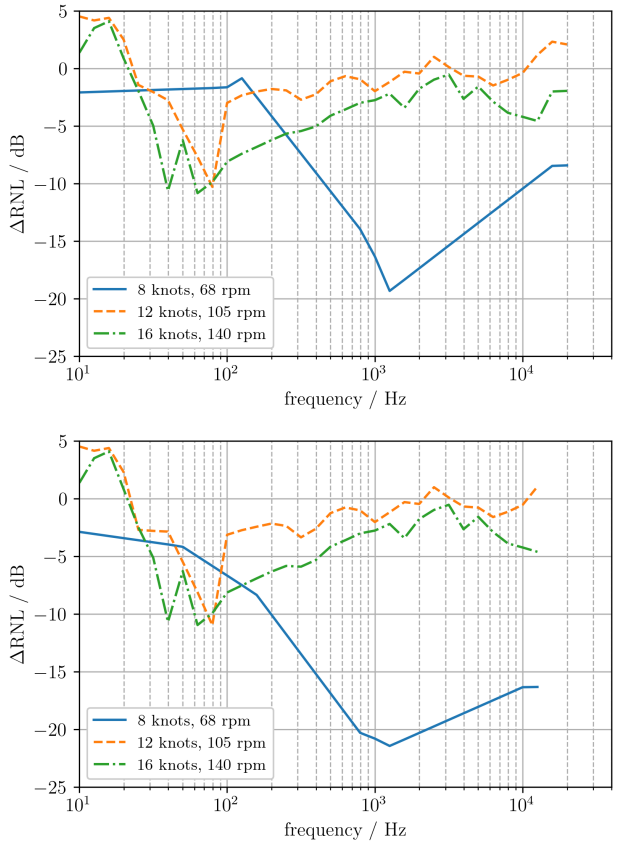

Figure 15: Comparison of change in radiated noise level for each of the three operating conditions considered: 'conservative' estimate (top); and 'optimistic' estimate (bottom).

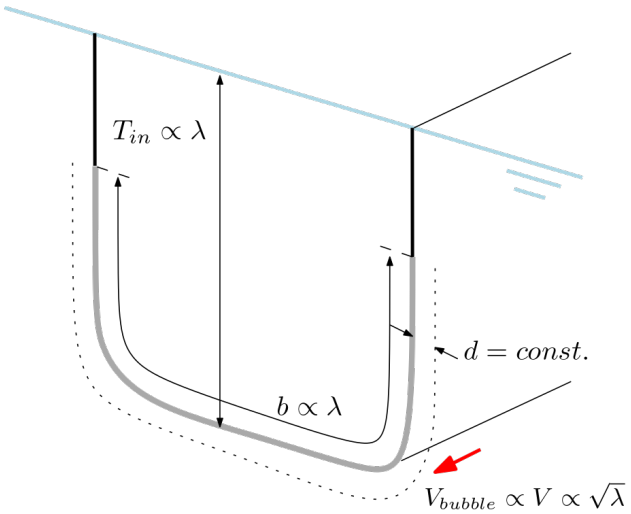

Figure 16: Schematic representations of Masker system used to derive scaling laws for air flow rate.

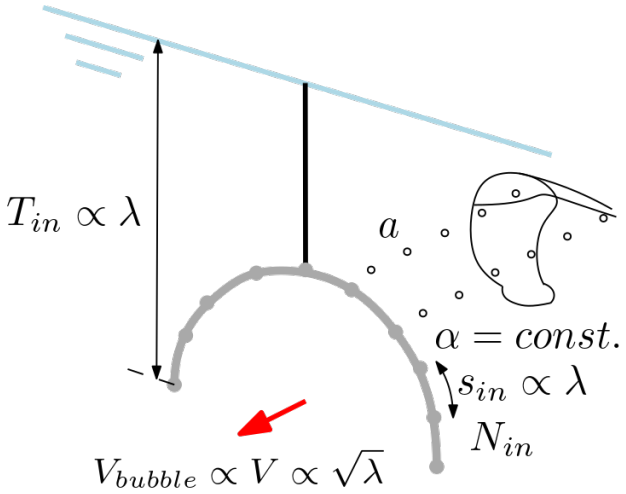

Figure 17: Schematic representations of Prairie-like system used to derive scaling laws for air flow rate.

For the Masker system, the required air flow rate is assumed to scale as:

$$Q \propto V \cdot b \cdot d \cdot \alpha, \tag{8}$$

while for the Prairie-like system this becomes:

$$Q \propto V \cdot N_{in} \cdot s_{in} \cdot a. \tag{9}$$

In Eq. 8, V is the forward speed, b the injector length in the girthwise direction, d the bubble layer thickness and α the air void fraction. In Eq. 9, N_{in} and s_{in} are the number of injectors and spacing between them respectively, while a is the bubble radius. These variables are also indicated in the schematics shown in Figures 16 and 17. In Eq. 9 we assume that it is possible to replace a with $\sqrt[3]{\langle V_a \rangle}$ where $\langle V_a \rangle$ is the mean air bubble volume and $\langle V_a \rangle \propto \alpha$. Furthermore, we do not account for changes in cavitation extents (propeller thrust coefficient or cavitation number) on the required flow rate, although this should be studied as part of future work. Applying Froude scaling in both cases, the ratio of the required air flow rates on ship- and model-scale becomes a function of the scale factor:

$$\frac{Q_s}{Q_m} = \begin{cases} \lambda^{1.5}, & \text{Masker} \\ \lambda^{2.5}, & \text{Prairie-like.} \end{cases} \tag{10}$$

It is also necessary to estimate the power requirement of the systems so that a suitable compressor can be selected. This is done here following Mäkiharju et al. (2012), who give the required compressor power as:

$$P_c = \frac{Q p_{atm} \gamma}{\eta_c (\gamma - 1)} \left[\left(\frac{p_{in}}{p_{atm}} \right)^{\frac{\gamma - 1}{\gamma}} - 1 \right], \tag{11}$$

where $p_{in} = p_{atm} + \rho g T_{in}$ is the static pressure at the injector and T_{in} is the draught at the injector(s). Table 3 summarises the results obtained using Eqs. 10 and 11. Overall, the power requirement is modest compared to other power demands on board (when considering typical installed auxiliary engine power for cargo vessels). Of course, the Prairie-like system requires much less air than the Masker system, since it is targeted at only part of the propeller disc compared to a relatively large section of the hull in the latter case.

Table 3: Air flow rates and required compressor power for ship scale application of Masker and Prairie-like systems, estimated from model-scale air flow rates.

System	Q_m / (m^3/s) $(\times 10^3)$	Q_m / (m^3/s) $(\times 10^6)$	Q_s / (m^3/s) $(\times 10^3)$	P_c / kW
Masker	6.25		260	24.8
Prairie-like		16.3	10	0.7
		25.0	15	1.0

4 DISCUSSION

Several points should be noted when interpreting the results presented, which also require further study.

One important aspect is how to apply the SLA data. This is due to the fact that the effect of the Prairie-like system is mainly to reduce the magnitude of the spectral hump caused by tip vortex cavitation, while in general also leading to an increase in source levels at (harmonics of) the blade passing frequency (BPF). Since the frequency of the hump peak is a function of the propeller design and loading condition (Bosschers 2018), the measured SLA spectrum is characteristic to the ship and propeller geometry used for the model tests, as well as the selected test conditions. Therefore the SLA data should not be applied to measurement data from other cases without shifting the maximum SLA to the correct peak frequency of the cavitation spectra hump, and the low-frequency negative SLA to the BPF, for the case being considered. Following Bosschers (2018), the peak frequency f_p can be estimated as:

$$\frac{f_p}{f_{bp}} \propto \frac{1}{\left(\frac{\tau K_T}{Z \sqrt{\sigma_n}} \right)} \frac{\sqrt{\sigma_n}}{Z} = \frac{\sigma_n}{\tau K_T}, \tag{12}$$

where $f_{bp} = nZ$ is the BPF, τ is a propeller maximum tip loading parameter, which models the effect of propeller design and hull form, and all other symbols have been previously defined. Applying Eq. 12 for the present case, a good agreement between the propeller rotation rate and loading condition was found between the M/V Overseas Harriette and the Streamline tanker, with the hump peak frequencies for the highest speed case being approximately equal to 50 Hz for both vessels. Based on this, no further adjustment of the SLA spectra was performed for the results shown here. However, it is expected that this will be necessary for other cases; for example, when a vessel has a much higher propeller rotation rate.

Another consideration relating to the Praire-like system is that the air injection can lead to a degradation in the propulsive performance of the propeller. This means that the model tests were not always performed at the self-propulsion condition. One way to correct for this effect is to estimate a new self-propulsion condition when the system is switched on, resulting in a change in rotation

rate, as well as associated propeller efficiency and URN source levels. For the results presented here, the maximum relative changes in rotation rate and propeller efficiency were estimated to be about +4 % and -5 % respectively. The accompanying change in SL can be predicted by rudimentary scaling as a function of propeller tip speed (e.g. see ITTC 2017) and was found to be about +1.5 dB. This serves to increase the expected absolute mitigated source levels in practice and has not been included in the analysis presented in Section 3. We expect that this effect can be minimised by reducing the amount of air injected through optimisation of the injector design to focus on the wake peak rather than the complete upper half of the duct. In addition, it may be possible to offset any change in propeller efficiency and/or source level by re-desiging the propeller using optimisation techniques, taking the application of a Prairie-like system into account.

One final point is the differences between the model tests and full-scale application in terms of ship motions, something which may affect the performance of both systems. Since the model tests were performed in ideal conditions, without any seaway modelled, no data is available on the relationship between ship motions and URN reduction. However, we might expect that (roll) motion would result in air escaping more quickly towards the free surface in the case of the Masker system, while for the Prairie-like system (time-varying) oblique inflow to the propeller may reduce the amount of air entering the cavity. This motivates additional model- or full-scale tests to study these effects.

5 CONCLUDING REMARKS

Exploratory model-scale tests of two air injection systems for mitigation of merchant ship URN were performed, with the aim of providing useful data for the design of quiet vessels. A brief overview of the model tests was presented, focusing in particular on how the URN measurements were analysed to quantify noise abatement potential. These results were then applied to measurement data for a real ship to demonstrate how they can be used in practice and what the expected reductions in URN could be. A method for estimating the power requirement of both systems was provided, since this is an additional design consideration.

For the Masker system an insertion loss of up to 22 dB was measured. This was obtained for the highest model speed and air flow rate used during the tests. In general, the IL showed a strong dependency on frequency. In the case of the Prairie-like system the maximum source level attenuation was about 12 dB, which occured around the centre frequency of the spectral hump caused by tip vortex cavitation. When combining these data in the ship-scale application case, the maximum change in radiated noise level was limited to around 10 dB, due to the relative contributions of the two source mechanisms.

The effect of limited or insufficient signal-to-noise ratio on the measured changes in source level in the model tests was discussed. Data fitting was required when addressing the ship-scale application case.

The procedure for applying the model test results to measurement data requires further development and formalisation; for example in how the SLA results should be applied on a case-by-case basis. This will be the subject of future work, which will also consider application to other cases, for different ship types than used here.

ACKNOWLEDGEMENTS

This work was carried out as part of the 'Developing Solutions for Underwater Radiated Noise' (SATURN) project: `https://www.saturnh2020.eu/`. SATURN has received funding from the European Union's Horizon 2020 research and innovation programme under grant agreement no. 101006443. We would like to thank our colleagues at MARIN who were involved in preparing, performing and analysing the model tests.

REFERENCES

Arveson, P. T. & Vendittis, D. J., 2000. 'Radiated noise characteristics of a modern cargo ship'. The Journal of the Acoustical Society of America, **107**(1), pp. 118–129.

Baudin, E. & Mumm, H., 2015. 'Guidelines for regulation on UW noise from commericial shipping (projects AQUO-SONIC)'. Tech. rep., Bureau Veritas and DNV GL. Publication Title: SONIC deliverable 5.4.

Bellmann, M. A., 2014. 'Overview of existing Noise Mitigation Systems for reducing Pile-Driving Noise'. Proceedings of Inter-noise 2014. 16th-19th November, Melbourne, Australia.

Bosschers, J., 2018. 'A semi-empirical prediction method for broadband hull-pressure fluctuations and underwater radiated noise by propeller tip vortex cavitation'. Journal of Marine Science and Engineering, **6**(2), p. 49.

Bosschers, J., Lafeber, F. H., de Boer, J., Bosman, R. & Bouvy, A., 2013. 'Underwater radiated noise measurements with a silent towing carriage in the depressurized wave basin'. Proceedings of 3rd International Conference on Advanced Model Measurement Technology. 17th-18th September, Gdansk.

Cruz, E., Lloyd, T., Lafeber, F., Bosschers, J., Vaz, G. & Djavidnia, S., 2022. 'The SOUNDS project: towards effective mitigation of underwater noise from shipping in Europe'. Proceedings of the Institute of Acoustics, **44**.

Duarte, C., Chapuis, L., Collin, S., Costa, D., Eguiluz, V., Erbe, C., Halpern, B., Havlik, M., Gordon, T., Merchant, N., Meekan, M., Miksis-Olds, J., Parsons, M., Predragovic, M., Radford, A., Radford, C., Simpson, S., Slabbekoorn, H., Staaterman, E., Opzeeland, I. V., Winderen, J., Zhang, X. & Juanes, F., 2021. 'The soundscape of the anthropocene ocean'. Science, **371**(583).

Dymarski, P., Salvatore, F., Pereira, F., Franchi, S. & Falchi, M., 2011. 'Results of model tests on reference configurations.' Tech. Rep. STREAMLINE-INS-DEL-

D21.1, INSEAN, Rome, Italy.

EU, 2017. 'Commission decision (EU) 2017/848 of 17 May 2017 laying down criteria and methodological standards on good environmental status of marine waters and specifications and standardised methods for monitoring and assessment, and repealing Decision 2010/477/EU'. Official Journal of the European Union, **125**(May), pp. 43–74.

Hadler, J. B., English, J. W. & Gupta, S. K., 1984. 'Program to minimize propeller-induced vibration on converted Maersk "E"-class ships'. SNAME, New York, USA.

IMO, 2023. 'Revised guidelines for the reduction of underwater radiated noise from shipping to address adverse impacts on marine life (MEPC.1/Circ.906)'. Tech. rep.

ITTC, 2017. 'Recommended procedures and guidelines. Model-scale propeller cavitation noise measurements'. Tech. rep., International Towing Tank Conference, Zurich, Switzerland. Publication Title: 7.5-02-01-05.

Joy, R., Tollit, D., Wood, J., MacGillivray, A., Li, Z., Trounce, K. & Robinson, O., 2019. 'Potential benefits of vessel slowdowns on endangered southern resident killer whales'. Frontiers in Marine Science, **6**, pp. 1–20.

Klinkenberg, Y., Bloemhof, F., Kamphof, H. J. & van Rijsbergen, M., 2023. 'Measuring air bubble layer characteristics around the hull of a ship model'. Proceedings of the 7th International Conference on Advanced Model Measurement Technology for the Maritime Industry. 24th-26th October, Istanbul, Turkey.

Krueger, S., Friesch, J. & Stoye, T., 2004. 'Reduction of propeller induced pressure fluctuations by systematic air injection'. Proceedings of 9th International Symposium on Practical Design of Ships and other Floating Structures. Luebeck-Travemuende, Germany.

Lloyd, T., Foeth, E.-J., Lafeber, F. H., Bosschers, J., Klinkenberg, Y., Birvalski, M., Kaydihan, L. & Lidtke, A., 2024. 'SATURN Deliverable 4.3. Impact of mitigation sources on source level of a single-screw vessel'. Technical report, Wageningen, The Netherlands.

Lloyd, T., Lafeber, F. H. & Bosschers, J., 2018. 'Investigation and validation of procedures for cavitation noise prediction from model-scale measurements'. Proceedings of 32nd Symposium on Naval Hydrodynamics. 5th-10th August, Hamburg, Germany.

Lloyd, T., Lafeber, F. H., Bosschers, J., Kaydihan, L. & Boerrigter, B., 2023. 'Scale model measurements of ship machinery noise mitigation by air injection'. Proceedings of 7th International Conference on Advanced Model Measurement Technology for the Maritime Industry. Istanbul, Turkey.

Mäkiharju, S. A., Perlin, M. & Ceccio, S. L., 2012. 'On the energy economics of air lubrication drag reduction'. International Journal of Naval Architecture and Ocean Engineering, **4**(4), pp. 412–422.

Technical Group on Underwater Noise, 2022. 'Setting of EU Threshold Values for continuous underwater sound. Marine Strategy Framework Directive (MSFD) Common Implementation Strategy'. Technical report.